

1       **Improving the high-cycle fatigue strength of heterogeneous carbon**  
2       **nanotube/Al-Cu-Mg composites through grain size design in**  
3       **ductile-zones**

4       K. Ma<sup>1,2</sup>, X.N. Li<sup>1</sup>, K. Liu<sup>2</sup>, X.G. Chen<sup>2</sup>, Z.Y. Liu<sup>1,\*</sup>, B.L. Xiao<sup>1,\*\*</sup>, Z.Y. Ma<sup>1</sup>

5       <sup>1</sup>Shi-changxu Innovation Center for Advanced Materials, Institute of Metal Research,  
6       Chinese Academy of Science, 72 Wenhua Road, Shenyang, 110016, China

7       <sup>2</sup>Department of Applied Science, University of Québec at Chicoutimi, Saguenay, Québec  
8       G7H 2B1, Canada

9       **Abstract:**

10       Heterogeneous structure consisting of brittle-zones (BZs) rich of carbon nanotubes (CNTs)  
11       and ductile-zones (DZs) free of CNTs, was an effective way to improve the  
12       strength-ductility of CNT reinforced Al (CNT/Al) composites. Two heterogeneous  
13       CNT/2009Al composites with coarse grain (CG, ~2 μm) DZs or ultra-fine grain (UFG,  
14       ~500 nm) DZs were fabricated and achieved enhanced strength-ductility. However, the  
15       heterogeneous composite with CG DZs had a lower high-cycle fatigue strength as well as  
16       fatigue strength/tensile strength ratio than the uniform composite, while the heterogeneous  
17       composite with UFG DZs exhibited the increased fatigue strength and the same level of  
18       fatigue strength/tensile strength ratio compared to the uniform composite. It was found  
19       that the improved fatigue properties for the heterogeneous composite with the UFG DZs  
20       could attribute to two reasons. Firstly, the UFG for the DZs significantly increased the  
21       strength of DZs, which effectively reduced the strain localization in the DZs. Secondly,  
22       the dislocations piling up at the grain boundaries of the BZs, as well as the stress

---

\*Corresponding author. E-mail address: zyliu@imr.ac.cn (Z.Y. Liu).

\*\*Corresponding author. E-mail address: blxiao@imr.ac.cn (B.L. Xiao).

1 concentration at the boundaries between the DZs and BZs were relieved due to the  
2 coordinated micro-strain for the heterogeneous structure. This provided a simple strategy  
3 for the structural design of heterogeneous composites with high fatigue strength.  
4 **Keywords:** A. Metal-matrix composites (MMCs); A. Carbon Nanotube; B. Fatigue; E.  
5 Powder processing

## 6 **1. Introduction**

7 With the continuous upgrading of high-tech equipment in aerospace, electronics,  
8 nuclear power and other fields, the demand for metal matrix composites (MMCs) with  
9 strong structural and performance designability, excellent physical and mechanical  
10 properties is growing rapidly [1-7]. Among them, carbon nanotube (CNT) reinforced Al  
11 matrix (CNT/Al) composites have attracted great attention due to their high specific  
12 strength, high specific modulus and good machinability [8-18]. However, the CNT/Al  
13 composites have a significant drawback of low ductility, which limits their industrial  
14 application. This is mainly due to the lower dislocation storability of the fine grains, and  
15 the strong pinning effect of CNTs on dislocation gliding [19-21].

16 The heterogeneous structures consisting of ductile-zones (DZs) and brittle-zones  
17 (BZs) by varied distribution of reinforcements or grain sizes, have been demonstrated as a  
18 promising approach to have a better trade off of the strength-ductility in ultrafine grained  
19 (UFG) metals and composites [22-28]. Recently, some scholars studied heterogeneous  
20 CNT/Al composites, and found that it had better strength-ductility than the uniform  
21 CNT/Al composite [29-34]. For example, Liu *et al.* [31] fabricated heterogeneous

1 CNT/Al-Cu-Mg composite by powder metallurgy method combined with subsequent hot  
2 extrusion, and reported that it achieved more than 100% elongation increase with nearly  
3 no loss of the tensile strength as compared to the uniform CNT/Al-Cu-Mg composite. The  
4 enhanced elongation was attributed to the greatly suppressed strain localization and  
5 effectively blunted micro-cracks due to the inhomogeneous structure. Meanwhile,  
6 geometrically necessary dislocations were induced between the DZs and BZs, leading to  
7 extra-strengthening beyond the rule-of-mixtures. On the basis of the toughening idea with  
8 heterogeneous structures, Tan *et al.* [34] fabricated heterogeneous CNT/Al-Cu-Mg  
9 composite with trimodal grain structure, and they were surprised to find that both the  
10 elongation and tensile strength of the heterogeneous composite were higher than that of  
11 the uniform composite. Tan's great achievement in heterogeneous CNT/Al composites  
12 further confirmed the beneficial role of tailoring grain structure in improving the  
13 toughness of CNT/Al composites.

14 For many industrial applications, the fatigue performance is a key criterion of  
15 structural materials. Therefore, it is of great importance to investigate the fatigue behavior.  
16 So far, the investigations of the heterogeneous materials were mainly focused on their  
17 tensile properties, investigations on the fatigue behaviors were quite rare. The fatigue  
18 behavior of the uniform CNT/Al composites was investigated in recent years [35, 36].  
19 Shin *et al.* [35] found that the addition of CNTs was helpful to improve the fatigue  
20 strength, which was mainly due to that the prevailing bridging behavior of CNTs  
21 suppressed the formation of catastrophic cracks. However, for the heterogeneous CNT/Al

1 composites, there was no related study on their fatigue behaviors.

2       According to the traditional view, the high-cycle fatigue (HCF) strength of the  
3 uniform materials was closely related to their static tensile strength, and the high static  
4 tensile strength usually corresponded to the high value of the fatigue strength [35, 37, 38].  
5 On the other hand, the fatigue cracks preferentially nucleated in the local deformation area,  
6 which deteriorated the fatigue properties. For example, Nelson *et al.* [39] found that the  
7 HCF cracks of the heterogeneous Al alloys nucleated in the low-strength coarse grained  
8 (CG) zones. Liu *et al.* [40] found that the HCF strength of the Cu-Al alloys mainly  
9 depended on the most vulnerable area within the inhomogeneous grain structure, and had  
10 less relation on the overall static mechanical properties. Therefore, it was generally  
11 believed that the inhomogeneous microstructure might not be good for the improvement  
12 of the fatigue properties. This poses a challenge for the application of heterogeneous  
13 composites under the fatigue conditions.

14       In recent years, some researchers found that the gradient materials with the grain  
15 transition from the nano-size at the sample surface to the micro-size at the sample center  
16 had the excellent fatigue properties. For example, Lu *et al.* [41] and Zhang *et al.* [42]  
17 fabricated Cu and TWIP steels with gradient grain structure respectively, and found that  
18 their HCF strengths were higher than those of CG and UFG counterparts. Qian *et al.* [43]  
19 studied the fatigue behavior of heterogeneous nickel with different grain sizes in the DZs,  
20 and found that the HCF strength was significantly improved as the grain size in the DZs  
21 was lower than 1  $\mu\text{m}$ , which was even higher than that of the uniform UFG nickel.

1 However, the mechanism of improving fatigue performance has not been well understood.  
2 It is not clear yet whether adjusting the grain size in the DZs could improve the fatigue  
3 performance of heterogeneous CNT/Al composites.

4 In this study, the heterogeneous CNT/Al composites with two different grain sizes in  
5 the DZs as well as the uniform CNT/Al composite were fabricated by powder metallurgy  
6 route. The fatigue performance and cyclic lives at different stress amplitudes were tested  
7 and the microstructures were analyzed. The aim is to (a) clarify the effect of  
8 heterogeneous structure on the fatigue properties, and (b) develop heterogeneous CNT/Al  
9 composites with high fatigue strength without reducing the strength-ductility.

## 10 **2. Experimental**

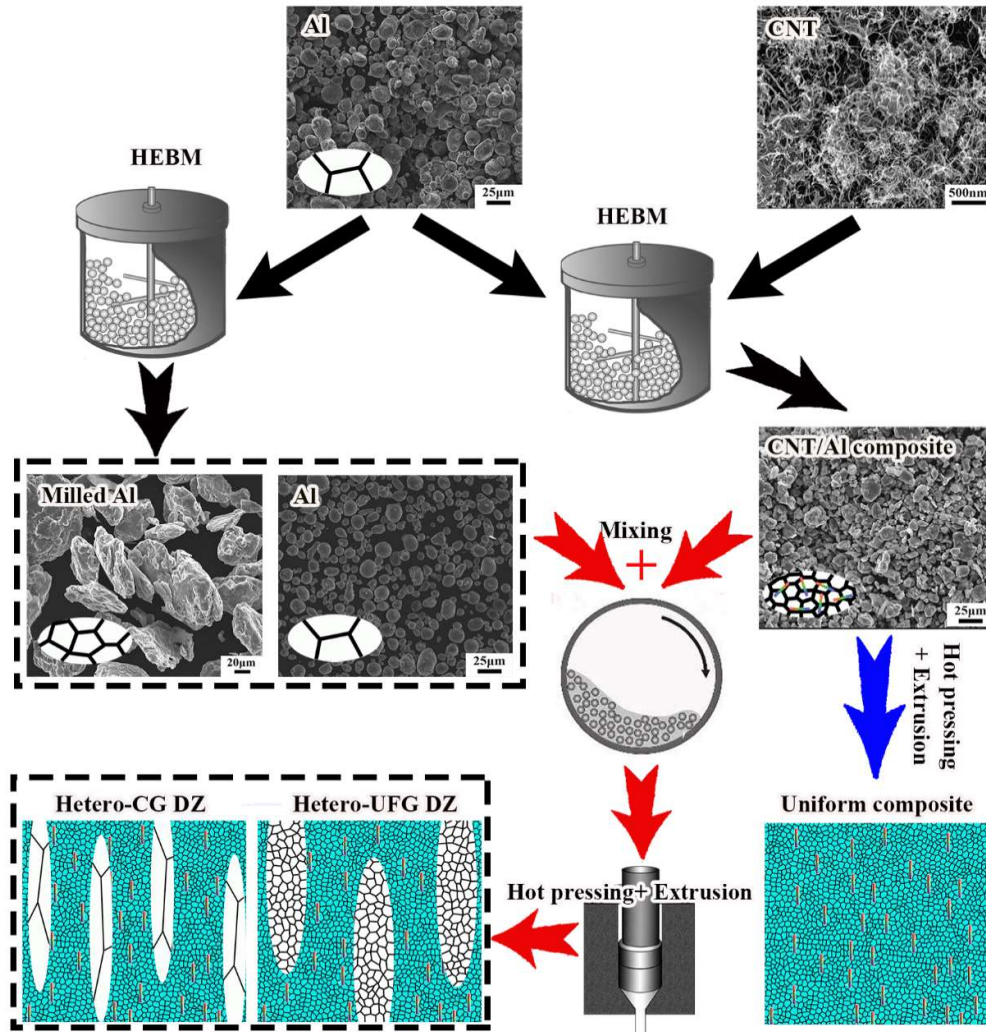
11 In the present work, CNT/Al composites with heterogeneous structures were  
12 fabricated through powder metallurgy routes, as shown in Fig. 1. Atomized 2009Al (Al-4  
13 wt.% Cu-1.5 wt.% Mg) powders with approximately 10  $\mu\text{m}$  diameters were used as raw  
14 metal materials. CNTs (~98% purity) fabricated by chemical vapor deposition had an  
15 outer diameter of 10-30 nm and a length of ~5  $\mu\text{m}$ . No extra pre-treatment was conducted  
16 on CNTs. 3 vol.% CNTs were high energy ball milled with 10  $\mu\text{m}$  as-received 2009Al  
17 powders at a rotation rate of 250 rpm with a ball to powder ratio of 15:1 for 10 h using an  
18 attritor, obtaining the milled CNT/2009Al composite powders.

19 In order to fabricate heterogeneous composites with different grain sizes in the DZs,  
20 two different 2009Al matrix powders, namely the as-received and the milled 2009Al  
21 powders were used, respectively. The milled 2009Al powders were obtained using high

1 energy ball milling (HEBM) process, which was similar that for the milled CNT/2009Al  
2 composite powders, but with the HEBM time of 4 h. 25% of these two matrix powders  
3 were respectively mixed with the ball milled CNT/2009Al composite powders using a  
4 dual axis mixer at a rotation rate of 50 rpm for 6 h, thereby obtaining two kinds of  
5 as-mixed heterogeneous composite powders.

6 The as-mixed composite powders were cold compacted and then vacuum hot pressed  
7 into billets under a pressure of 50 MPa at 813 K. The billets were extruded into bars at 743  
8 K with an extrusion ratio of 16:1. The extruded bars were solution treated at 770 K for 2 h,  
9 quenched into water and naturally aged for 4 days (T4 state). For convenience, the final  
10 heterogeneous composites prepared by mixing the milled composite powders with  
11 as-received or milled 2009Al alloy powders were respectively abbreviated as Hetero-CG  
12 DZ and Hetero-UFG DZ.

13 For comparison, the uniform 2.25 vol.% CNT/2009Al composite was also fabricated.  
14 The fabrication process was similar to that for the heterogeneous CNT/2009Al composites,  
15 but no additional 2009Al matrix powders were mixed with the milled CNT/2009Al  
16 composite powders. The uniform 2.25 vol.% CNT/2009Al composite was simplified as  
17 Uniform composite.



1

2

3 **Fig. 1** Schematic of the fabrication process of CNT/2009Al composites with  
 4 heterogeneous and uniform structures.

5

6

7

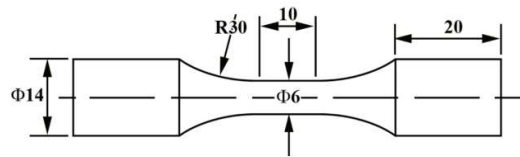
8

9

10

The samples with T4 state for tensile and fatigue testing were machined from the extruded bars with the axis parallel to the extrusion direction, and the dimension of the fatigue sample is shown in Fig. 2. HCF tests were performed using servo-hydraulic facility equipment (Instron 8801 tester) under the load-controlled mode at a frequency of 20 Hz and a stress ratio of  $R = \sigma_{\min}/\sigma_{\max} = 0.1$  ( $\sigma_{\min}$  and  $\sigma_{\max}$  are the minimum and maximum applied stresses, respectively) at room temperature. The microstructures were

1 characterized by optical microscopy (OM; Zeiss Axiovert 200 MAT), scanning electron  
2 microscopy (SEM; JSM-6480LV) and transmission electron microscopy (TEM;  
3 JEM-2100). The TEM samples for observing the initial microstructure were cut from the  
4 extruded bars with the foil plane parallel to the extrusion direction, and the TEM samples  
5 for observing the microstructure after fatigue were cut from the fatigue samples near the  
6 fracture surface, with the foil plane vertical to the loading direction. All the thin foils for  
7 TEM were ground to a thickness of 60  $\mu\text{m}$ , punched to disks with a diameter of 3 mm,  
8 then dimpled to a minimum thickness of 20  $\mu\text{m}$  and finally ion-beam thinned by a Gatan  
9 Model 691 ion milling system.



10  
11 **Fig. 2** The drawing of the fatigue sample (all dimensions in mm).

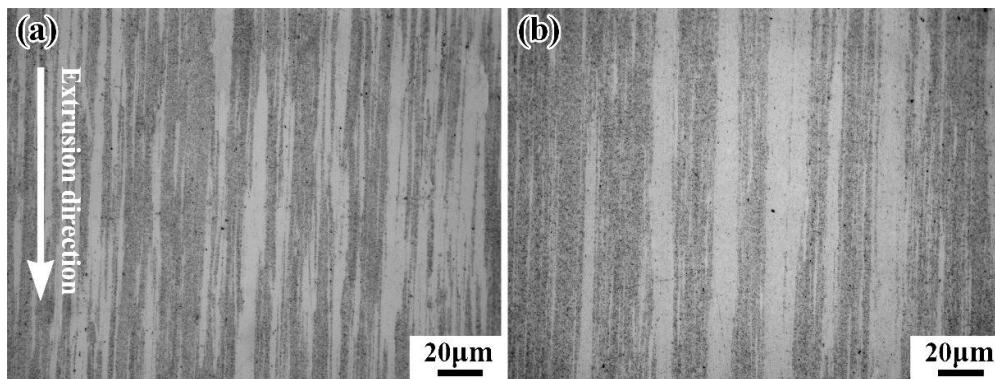
### 12 **3. Results and discussion**

#### 13 **3.1 Initial microstructure**

14 Fig. 3 shows the OM images of the two kinds of heterogeneous CNT/2009Al  
15 composites. It can be seen that the bright zones aligned along the extrusion direction were  
16 embedded in the dark zones. According to our previous investigations [30-32], the bright  
17 zones were the DZs originating from the additional matrix powders, and the dark zones  
18 were the BZs originating from the milled CNT/Al composite powders. The DZ bands for  
19 the Hetero-CG DZ were slightly thinner (Fig. 3(a)) than those of the Hetero-UFG DZ (Fig.  
20 3(b)). According to the dimension statistical analysis of at least 100 DZ bands for each



1 composite, the average DZ band widths of the Hetero-CG DZ and Hetero-UFG DZ were  
2 measured to be 2.6 and 6.6  $\mu\text{m}$ , respectively. The difference in the DZ bands between the  
3 Hetero-UFG DZ and Hetero-CG DZ was mainly caused by the different dimensions of the  
4 additional mixed 2009Al powders. For the Hetero-UFG DZ, the added 2009Al powders  
5 went through 4 h HEBM process. The cold-welding between the powders during the  
6 HEBM process led to the increase of the powder dimension, so the DZ width of the  
7 Hetero-UFG DZ was larger than that of the Hetero-CG DZ.

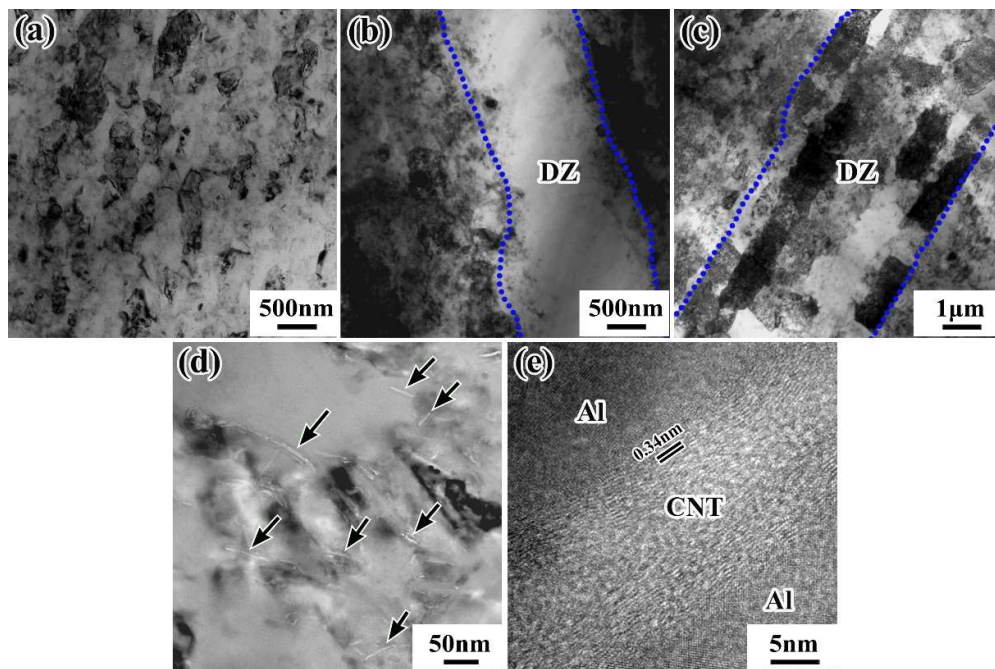


8  
9 **Fig. 3** OM images of BZ and DZ morphologies in the heterogeneous composites: (a)  
10 Hetero-CG DZ and (b) Hetero-UFG DZ.

11 Fig. 4 shows the TEM images of grain morphologies and CNT distribution in  
12 different CNT/2009Al composites. It can be seen that the grains in the Uniform composite  
13 were very small, with the average grain size of  $\sim 200$  nm (Fig. 4(a)). For heterogeneous  
14 composites, their grain morphologies in the BZs of the two heterogeneous composites  
15 were similar with that of the Uniform composite. CNTs with average length of  $\sim 100$  nm  
16 (marked by black arrows) were uniformly distributed in the BZs (Fig. 4(d)). High  
17 resolution TEM image indicates that the interface between CNT and Al matrix was well

1 bonded, and the structure integrity of CNTs maintained well (Fig. 4(e)).

2 However, the grain morphologies in the DZs of these two heterogeneous composites  
3 were quite different. For the Hetero-CG DZ, the grain width in the DZs was  $\sim 2 \mu\text{m}$ , and  
4 the grain length was larger than  $5 \mu\text{m}$  (Fig. 4(b)). For the Hetero-UFG DZ, the grains in  
5 the DZs were significantly refined, with the average grain width of  $\sim 500 \text{ nm}$  and the grain  
6 length of  $\sim 2 \mu\text{m}$  (Fig. 4(c)). The refined grains in the DZs for the Hetero-UFG DZ was  
7 caused by the severe plastic deformation during the HEBM process.

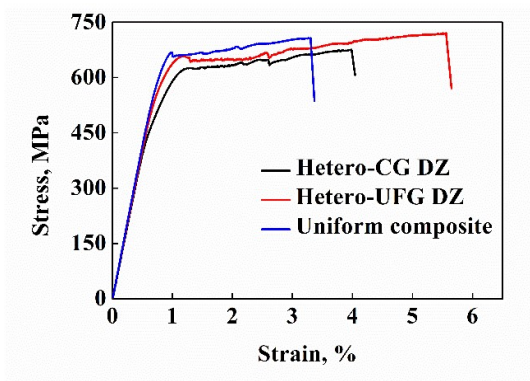


8  
9 **Fig. 4** TEM images of (a) Uniform composite, (b) Hetero-CG DZ, (c) Hetero-UFG DZ  
10 (Blue lines in (b) and (c) are the boundaries between the DZs and BZs), (d) CNT  
11 distribution (indicated by black arrows) and (e) High resolution TEM image showing  
12 CNT-Al interface in the BZs.

### 13 3.2 Tensile and high-cycle fatigue properties

14 Tensile stress-strain curves for the Uniform composite, Hetero-CG DZ and  
15 Hetero-UFG DZ are shown in Fig. 5. The Uniform composite had a high yield strength

1 (YS) of 671 MPa and a high ultimate tensile strength (UTS) of 707 MPa, but the  
 2 elongation (El) was as low as 2.5%. Compared with the Uniform composite, the both  
 3 heterogeneous composites exhibited a much higher strength ductility product (UTS×El),  
 4 which demonstrates an enhanced strength-ductility of the heterogeneous structure. All the  
 5 mechanical and fatigue properties are listed in Table 1. By comparing the tensile  
 6 properties of two heterogeneous composites, it can be seen that all the tensile properties  
 7 (including the YS, UTS and El) of the Hetero-UFG DZ were higher than that of the  
 8 Hetero-CG DZ, which demonstrates that the strength-ductility of the Hetero-UFG DZ was  
 9 better than that of the Hetero-CG DZ.



10

11 **Fig. 5** Tensile properties of the uniform and heterogeneous composites.

12 **Table 1** Mechanical and fatigue properties of the three CNT/2009Al composites with  
 13 different structures.

| Sample            | Tensile properties |           |         |                             | Fatigue properties  |      |
|-------------------|--------------------|-----------|---------|-----------------------------|---------------------|------|
|                   | YS (MPa)           | UTS (MPa) | El (%)  | UTS×El (MJ/m <sup>3</sup> ) | $\sigma_{FS}$ (MPa) | $m$  |
| Uniform composite | 671±5              | 707±5     | 2.5±0.2 | 16.7                        | 450                 | 0.64 |
| Hetero-CG DZ      | 574±5              | 680±8     | 3.8±0.5 | 25.8                        | 420                 | 0.62 |
| Hetero-UFG DZ     | 620±7              | 720±6     | 4.7±0.5 | 33.8                        | 460                 | 0.64 |

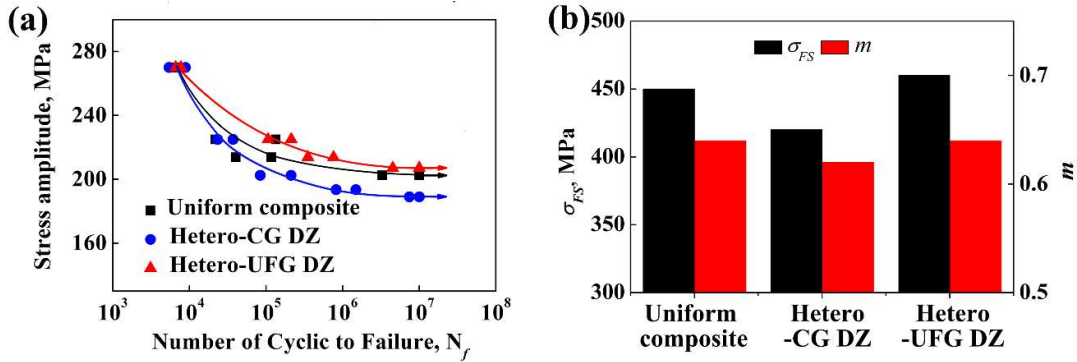
1        The stress amplitudes versus the numbers of cycles-to-failure ( $N_f$ ) are shown in Fig.  
2 6(a), and the arrows indicate that the specimens did not fail. Similar to that for most of  
3 other materials, the fatigue life of the composites decreased as the applied stress increased.  
4 At a certain  $N_f$ , the stress amplitude of the Hetero-CG DZ, Uniform composite and  
5 Hetero-UFG DZ increased in turn, which indicates the Hetero-UFG DZ exhibited the best  
6 fatigue performance. As the  $N_f$  reaches to  $10^6\sim 10^7$  cycles, the corresponding maximum  
7 stress can be determined as fatigue strength  $\sigma_{FS}$  [44]. In general, high ultimate tensile  
8 strength  $\sigma_{UTS}$  usually leads to a high fatigue strength [45]. The ratio of  $\sigma_{FS}$  to  $\sigma_{UTS}$   
9 could be given by Eq. 1 [35]:

$$10 \qquad m = \sigma_{FS} / \sigma_{UTS} \qquad (1)$$

11        The value of  $m$ , a parameter determined from the experimental data for many metallic  
12 materials such as iron, copper, and Al alloys, has been well established. According to a  
13 large number of fatigue data for these materials,  $m$  are estimated to be 0.4~0.6 for steels  
14 and Al alloys [44, 46]. As shown in Fig. 6(b) and Table 1, all the composites had a high  $m$ ,  
15 which was higher than 0.6. However, the  $m$  of Hetero-CG DZ was lower than that of other  
16 two composites.

17        The high fatigue strength and high  $m$  value of the uniform CNT/Al composites were  
18 reported by Shin *et al.* [35]. They found that the more CNT content led to the higher  
19 fatigue strength and  $m$  value. The enhanced fatigue performance was mainly attributed to  
20 that the prevailing bridging behavior of CNTs could inhibit the propagation of cracks. In  
21 the present work, all the three composites had the same CNT content of 2.25 vol.%,

1 expecting the similar influence of CNTs on high fatigue strength and  $m$  value. Therefore,  
 2 the different fatigue strength and  $m$  should be related to the CNT distribution and  
 3 heterogeneous structure, which will be discussed in the next section.



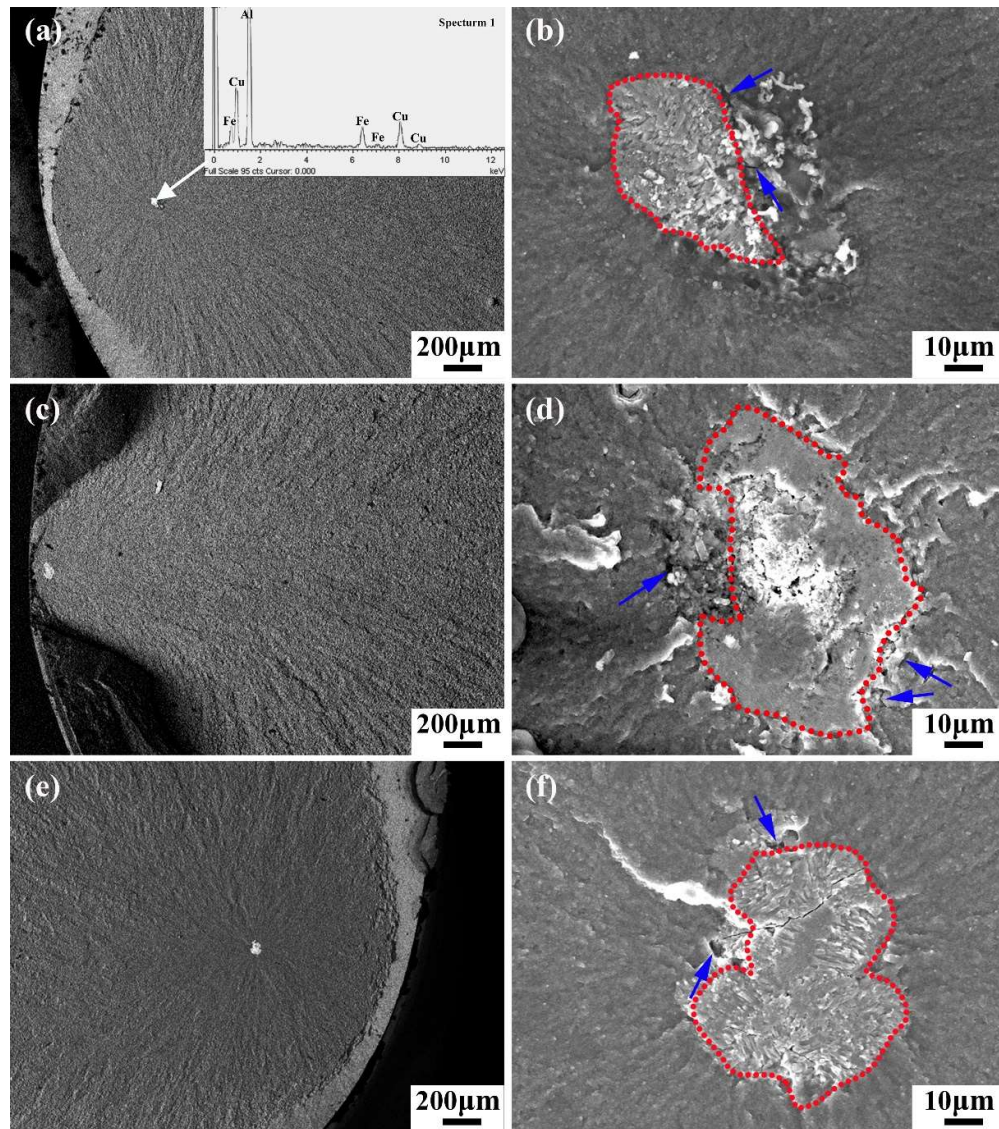
4  
 5 **Fig. 6** (a) Stress amplitude versus the number of cyclic to failure curve, (b)  $\sigma_{FS}$  and  $m$  for  
 6 different composites.

### 7 3.3 Fractograph analysis

8 Fig. 7 shows the typical crack initiation sites for different composites. It can be found  
 9 that all the three composites had the similar crack nucleation feature that the radial  
 10 striations converged at the inclusion near the surface of the specimens (Fig. 7(a)(c)(e)).  
 11 The inclusion size was approximately 30 to 50  $\mu\text{m}$ , and some voids or micro-cracks  
 12 (marked by arrows) were observed at the interfaces between the inclusion and matrix (Fig.  
 13 7(b)(d)(f)). All the inclusions were determined to be rich in Fe by SEM-energy dispersive  
 14 spectrometry. That is, fatigue crack nucleation of all the three composites took place at  
 15 Fe-rich inclusions near the specimen surface.

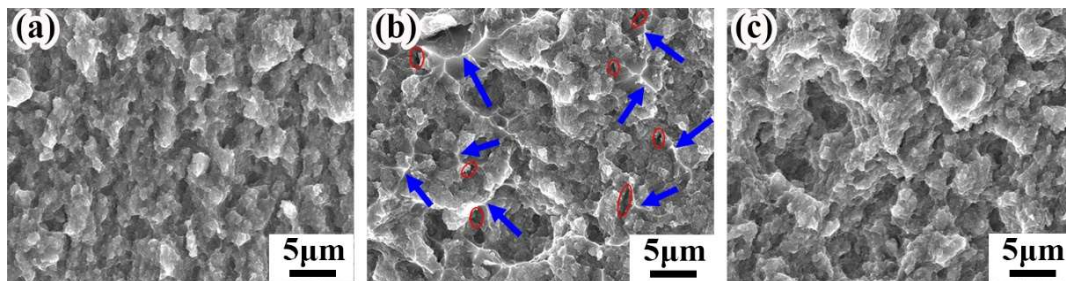
16 Since CNTs were dispersed into the matrix powders by the HEBM method, after a  
 17 long period of severe collision, the steel balls would inevitably introduce some impurities

1 such as steel filings into the powders. As the powders were hot-consolidated at elevated  
2 temperature, Fe-rich inclusions formed [47]. The Fe-rich inclusions as the fatigue crack  
3 initiation were also widely reported in other Al alloys and Al matrix composites [48, 49].



4  
5 **Fig. 7** SEM images showing the fatigue crack initiation sites on the fracture surfaces of  
6 (a)(b) Uniform composite (stress amplitude of 203 MPa,  $3.3 \times 10^6$  cycles to failure), (c)(d)  
7 Hetero-CG DZ (stress amplitude of 189 MPa,  $7.4 \times 10^6$  cycles to failure), (e)(f)  
8 Hetero-UFG DZ (stress amplitude of 207 MPa,  $4.5 \times 10^6$  cycles to failure) (Red circles  
9 indicate the Fe-rich inclusions and blue arrows indicate the voids).

1 Fig. 8 shows the fractograph away from the specimen surfaces. No obvious fatigue  
2 striations were observed in all the three specimens, which indicates rapid fracture occurred  
3 after crack initiation. For the Uniform composite, the dimples were small (Fig. 8(a)), while  
4 the dimples were a little larger for the heterogeneous composites (Fig. 8(b)(c)).  
5 Furthermore, many tear ridges (marked by blue arrows) were found within the Hetero-CG  
6 DZ. No CNTs could be found in the tear ridges, referring that the tear ridges were formed  
7 by the DZs. Some micro-cracks (marked by red circles) distributed at the edges of the tear  
8 ridges in the Hetero-CG DZ as shown in Fig. 8(b), indicating that there were stress  
9 concentrations at the boundaries between the DZs and BZs. The occurrence of stress  
10 concentration should be responsible for the low fatigue strength and  $m$  of the Hetero-CG  
11 DZ.

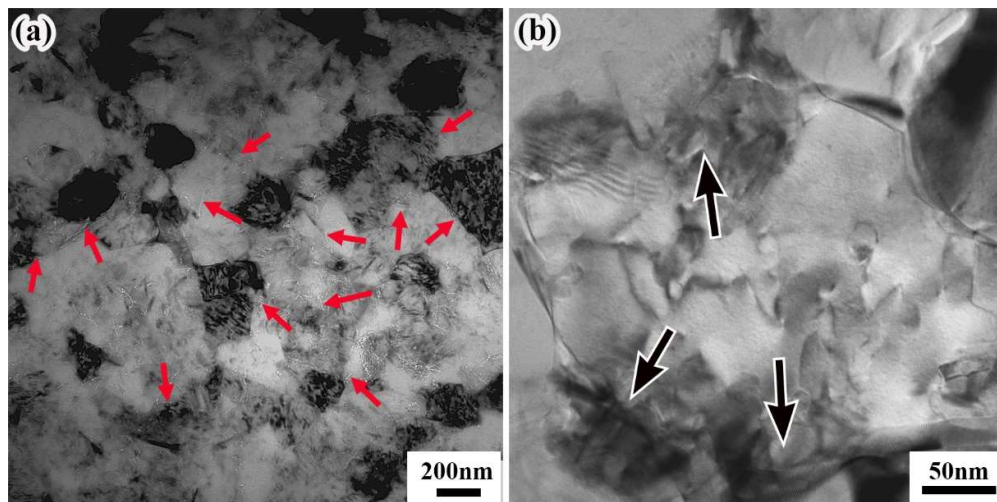


12  
13 **Fig. 8** Fracture morphologies at the center of the samples: (a) Uniform composite (stress  
14 amplitude of 203 MPa,  $3.3 \times 10^6$  cycles to failure), (b) Hetero-CG DZ (stress amplitude of  
15 189 MPa,  $7.4 \times 10^6$  cycles to failure), (c) Hetero-UFG DZ (stress amplitude of 207 MPa,  
16  $4.5 \times 10^6$  cycles to failure) (Red circles indicate the micro-cracks and blue arrows indicate  
17 the tear ridges).

### 18 3.4 Damage mechanism

19 Fig. 9 displays the TEM images of the Uniform composite after fatigue test. It can be  
20 seen that the grain size still retained as small as about 200 nm, while CNTs were

1 uniformly distributed within the matrix (marked by red arrows in Fig. 9(a)). The  
2 phenomenon of stable grain size after fatigue test for the UFG composites was quite  
3 different from that for the UFG Al alloys [38, 50]. Goswami *et al.* [50] reported that UFG  
4 Al would coarsen after fatigue test, because the adjacent fine grains tended to align under  
5 cyclic stress. For the CNT/Al composites, a large number of CNTs were embedded in the  
6 matrix, which had a strong pinning effect on grain boundaries (GBs) and would prohibit  
7 the grain growth during the fatigue testing, leading to the stable grain size. Meanwhile,  
8 according to the Hall-Petch relationship, the smaller grain size led to the higher strength  
9 [19]. Therefore, the stable and small grain size would be responsible for the high fatigue  
10 strength and  $m$  of the Uniform composite.



11  
12 **Fig. 9** TEM images of the Uniform composite after fatigue test (stress amplitude of 203  
13 MPa,  $3.3 \times 10^6$  cycles to failure): (a) grain and CNT distribution (CNTs indicated by red  
14 arrows), (b) dislocation morphology (Black arrows indicate the dislocations piling up at  
15 the GBs).

16 The magnified image of the UFG indicates that some entangled dislocations were

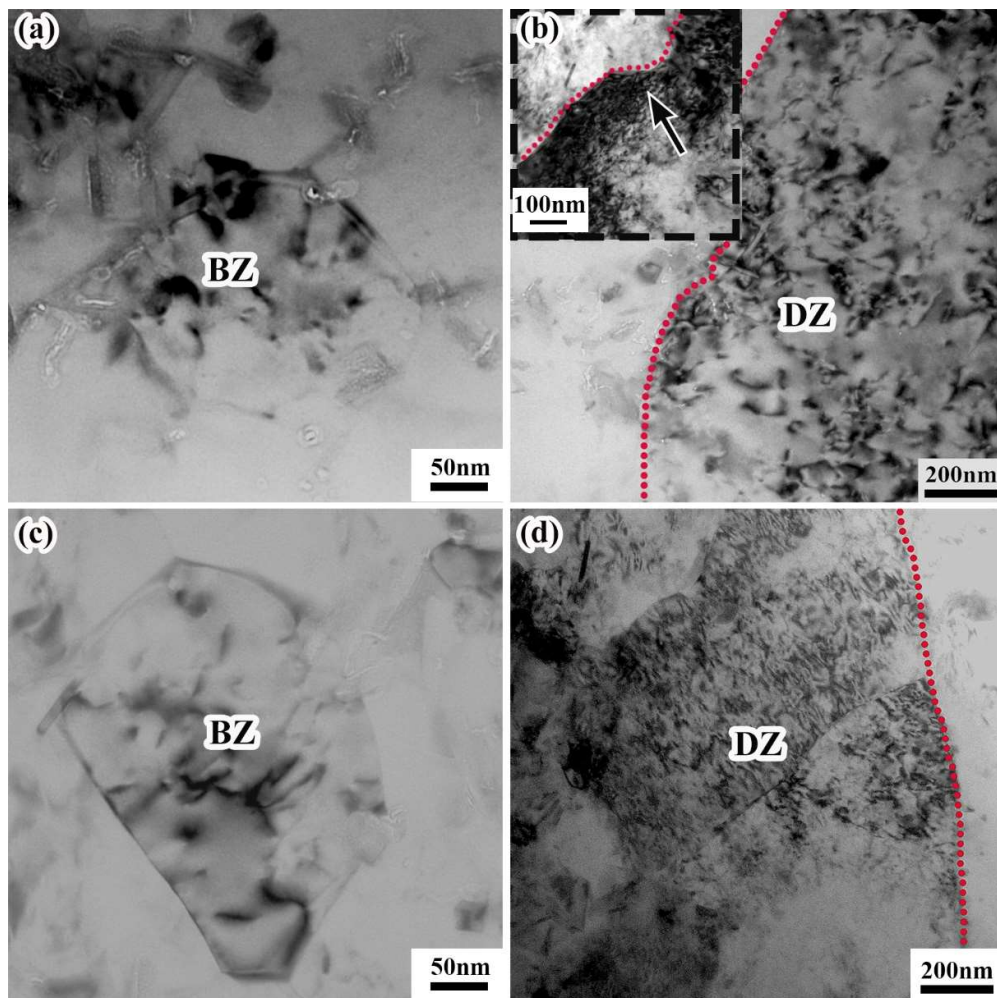


1 formed within the grains, and dislocations piled up at the GBs (marked by black arrows in  
2 Fig. 9(b)). It is well known that the boundaries as a barrier can inhibit the movement of  
3 dislocations, and the piled-up dislocations will further develop into micro-crack defects  
4 under cyclic loading [51]. Therefore, the failure mode of the Uniform composite could be  
5 inferred that the dislocation piling up at the GBs promoted the crack nucleation and then  
6 the cracks propagated to cause the material failure.

7 Fig. 10 shows the TEM images of the heterogeneous composite specimens after  
8 fatigue test. For the Hetero-CG DZ, a small number of dislocations can be observed within  
9 the grains of BZs, and no obvious piled-up dislocations were observed at the GBs (Fig.  
10 10(a)). Compared with that of the Uniform composite, the reduced dislocation density in  
11 the BZs of the Hetero-CG DZ could attribute to the more deformation in the low-strength  
12 DZs. This could be reflected in the TEM image of DZs in the Hetero-CG DZ (Fig. 10(b)).  
13 A large number of dislocations could be observed in the DZs, indicating the preferential  
14 deformation in the DZs. Nelso *et al.* [39] investigated the HCF behavior of the  
15 heterogeneous Al alloys. They found that the DZs with lower strength preferentially  
16 deformed, and the fatigue life of the heterogeneous Al alloys was lower than that of the  
17 uniform counterpart. The low fatigue strength of the Hetero-CG DZ in the present study  
18 agreed well with the Nelso's investigation.

19 In addition to reducing the overall strength of the material by mixing the low-strength  
20 CG DZs, the stress concentration at the boundaries between the DZs and BZs that would  
21 accelerate the fatigue damage was also an important reason to decrease the fatigue

1 strength. As shown by the black arrow inside of Fig. 10(b), a large number of dislocations  
2 were accumulated at the boundaries between the DZs and BZs, indicating the serious  
3 stress concentration at the boundaries between the DZs and BZs. This was in accordance  
4 with the fractograph as shown in Fig. 8(b), where there were many cracks at the edge of  
5 the DZs. Because the significant stress concentration would promote crack nucleation, the  
6  $m$  would also be low. On the whole, both the addition of low-strength CG DZs and the  
7 stress concentration at the boundaries between the DZs and BZs would decrease the  $\sigma_{FS}$  of  
8 the Hetero-CG DZ.



9  
10 **Fig. 10** TEM images of (a)(b) the Hetero-CG DZ after fatigue test (stress amplitude of 189

1       MPa,  $7.4 \times 10^6$  cycles to failure), (c)(d) the Hetero-UFG DZ after fatigue test (stress  
2       amplitude of 207 MPa,  $4.5 \times 10^6$  cycles to failure) (Red lines are the boundaries between  
3       the DZs and BZs).

4       For the Hetero-UFG DZ, a few dislocations could be observed within the grains in  
5       the BZs, and no obvious piled-up dislocations were observed at the GBs (Fig. 10(c)).  
6       However, the dislocation distribution in the DZs for the Hetero-UFG DZ was quite  
7       different from that for the Hetero-CG DZ, the dislocations only occurred at some parts of  
8       the DZs (Fig. 10(d)). This was because that the DZs contained many grains in the  
9       Hetero-UFG DZ, dislocations tended to move within the crystal plane that facilitates  
10      slipping. Due to the different crystal orientations between adjacent grains in the DZs, the  
11      continuous movement of dislocations would be interrupted at the GBs. The deformation  
12      concentration area in the DZs was divided into multiple smaller-sized units by the inner  
13      GBs, so the deformation concentration in the DZs would be weakened. Further, the grains  
14      of the DZs were refined by HEBM, which reduced the grain size difference between the  
15      DZs and BZs, and further relaxed the stress concentration at the boundaries between the  
16      DZs and BZs. The grain refinement in the DZs led to the increase of the strength and the  
17      decrease of the stress concentration, resulting in the enhanced fatigue properties (including  
18      the  $\sigma_{FS}$  and  $m$ ) of the Hetero-UFG DZ, as compared with those of the Hetero-CG DZ.

19      It should be mentioned that, the  $m$  of the Hetero-UFG DZ was the same as that of the  
20      Uniform composite and the  $\sigma_{FS}$  of the Hetero-UFG DZ was even slightly higher than  
21      that of the Uniform composite. The high  $m$  of the Hetero-UFG DZ was believed to result  
22      from the following two reasons. On one hand, the grain size difference between the DZs

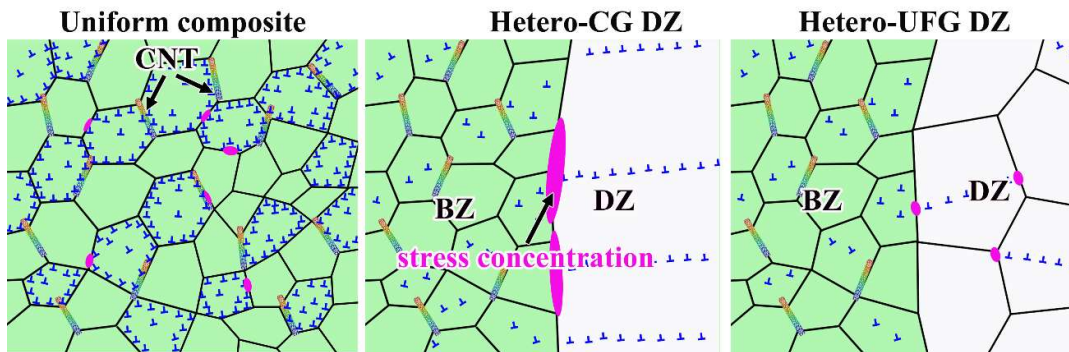
1 and BZs was very small, so the stress concentration at the boundaries between the DZs  
2 and BZs could be easily relaxed. On the other hand, the dislocations piling up at the  
3 boundaries of the BZs were relieved due to the coordinated micro-strain for the  
4 heterogeneous structure, which extended the life time of the BZs. Finally, because the  
5 Hetero-UFG DZ had the higher UTS and the same  $m$  as the Uniform composite, the  $\sigma_{FS}$   
6 of the Hetero-UFG DZ would be higher than that of the Uniform composite.

7       The damage mechanism of the uniform and heterogeneous CNT/2009Al composites  
8 under the cycle loading can be schematically summarized in Fig. 11. For the Uniform  
9 composite, the GBs were pinned by CNTs and no obvious grain coarsening could be  
10 observed. Under the fatigue stress, dislocations slipped inside the grains and piled up at  
11 the GBs. As the cycle number increased, the dislocations piling up at the GBs increased,  
12 and eventually cracks nucleated at the GBs, resulting in fatigue fracture.

13       For the Hetero-CG DZ, due to the introduction of the CGs in the DZs with lower  
14 strength, the cyclic deformation preferred to develop in the DZs, so the dislocation  
15 distribution in the DZs was much denser than that in the BZs. Because the deformation  
16 portion in the BZs was reduced, the dislocation accumulation at the GBs in the BZs  
17 became weaker. However, due to the large deformation mismatch between the DZs and  
18 BZs, the stress concentration at the boundaries between the DZs and BZs was severe, and  
19 microcracks were also easy to nucleate at the boundaries between the DZs and BZs. With  
20 the addition of low-strength DZs and significant stress concentration at the boundaries  
21 between the DZs and BZs, the fatigue properties of the Hetero-CG DZ were the weakest

1 among the three composites.

2 For the Hetero-UFG DZ, the grain size in the DZs was much smaller as compared  
3 with that for the Hetero-CG DZ, which resulted in a higher strength of the DZs. Because  
4 the grain size difference between the BZs and DZs was quite small, the stress  
5 concentration at the boundaries between the DZs and BZs in the Hetero-UFG DZ was  
6 much lower than that in the Hetero-CG DZ. Furthermore, the strain localization in the BZs  
7 was decreased due to the heterogeneous structure. As a result, the  $\sigma_{FS}$  of the Hetero-UFG  
8 DZ was the highest among the three composites and the  $m$  of the Hetero-UFG DZ was as  
9 high as that of the Uniform composite.



10  
11 **Fig. 11** Schematic illustration of deformation behavior and damage mechanism of the  
12 three CNT/2009Al composites (Uniform composite, Hetero-CG DZ and Hetero-UFG DZ).

#### 13 4. Conclusions

14 In this study, the uniform and two kinds of heterogeneous CNT/2009Al composites  
15 with different grain sizes in the DZs were fabricated by powder metallurgy routes. The  
16 high cycle fatigue tests with the stress ratio of 0.1 and frequency of 20 Hz were carried out,  
17 and the microstructures before and after fatigue test were analyzed. The following  
18 conclusions can be drawn:

1 (1) All the three CNT/2009Al composites, including the uniform composite, the  
2 heterogeneous composite with coarse grain ductile-zones and the heterogeneous  
3 composite with ultrafine grain ductile-zones exhibited high fatigue strength/tensile  
4 strength ratio ( $m$ ), with  $m$  values of 0.64, 0.62 and 0.64, respectively.

5 (2) For the heterogeneous composites with coarse grained ductile-zones, the fatigue  
6 strength was lower than that of the uniform composite, due to the introduction of  
7 low-strength coarse grain ductile-zones and significant stress concentration at the  
8 boundaries between the ductile-zones and brittle-zones.

9 (3) The ultra-fine grain of the ductile-zones could effectively increase the strength of  
10 the ductile-zones. The ultra-fine grain of the ductile-zones also reduced the grain  
11 difference between brittle-zones and ductile-zones, which relaxed the stress concentration  
12 at the boundaries between the ductile-zones and brittle-zones. Further, the heterogeneous  
13 structure could reduce the dislocations piling up at grain boundaries in the brittle-zones.  
14 As a result, the fatigue strength of the heterogeneous composite with the ultra-fine grain  
15 ductile-zones was higher than that of the uniform composite while maintaining its good  
16 strength-ductility.

## 17 **Acknowledgements**

18 This work was supported by: (a) Key R&D Program of China under grant (No.  
19 2017YFB0703104); (b) Key Research Program of Frontier Sciences, CAS (NO.  
20 QYZDJ-SSW-JSC015); (c) National Natural Science Foundation of China (No. 51871215,  
21 No. 51931009, No.51871214); (d) the Youth Innovation Promotion Association CAS

1 (2020197). K. Ma would like to acknowledge the support from China Scholarship  
2 Council.

### 3 **References**

- 4 [1] Xiao BL, Huang ZY, Ma K, Zhang XX, Ma ZY. Research on Hot Deformation  
5 Behaviors of Discontinuously Reinforced Aluminum Composites. *Acta Metall Sin.*  
6 2019;55(1):59-72.
- 7 [2] Ma K, Zhang XX, Wang D, Wang QZ, Liu ZY, Xiao BL, et al. Optimization and  
8 Simulation of Deformation Parameters of SiC/2009Al Composites. *Acta Metall Sin.*  
9 2019;55(10):1329-37.
- 10 [3] Liu J, Fan G, Tan Z, Guo Q, Su Y, Li Z, et al. Mechanical properties and failure  
11 mechanisms at high temperature in carbon nanotube reinforced copper matrix  
12 nanolaminated composite. *Composites Part A.* 2019;116:54-61.
- 13 [4] Zan YN, Zhou YT, Zhao H, Liu ZY, Wang QZ, Wang D, et al. Enhancing  
14 high-temperature strength of (B<sub>4</sub>C+Al<sub>2</sub>O<sub>3</sub>)/Al designed for neutron absorbing materials by  
15 constructing lamellar structure. *Composites Part B.* 2020;183:107674.
- 16 [5] Liu ZY, Wang LH, Zan YN, Wang WG, Xiao BL, Wang D, et al. Enhancing  
17 strengthening efficiency of graphene nano-sheets in aluminum matrix composite by  
18 improving interface bonding. *Composites Part B.* 2020;199:108268.
- 19 [6] Zhu SZ, Wang D, Xiao BL, Ma ZY. Suppressed negative effects of natural aging by  
20 pre-aging in SiCp/6092Al composites. *Composites Part B.* 2021;212:108730.
- 21 [7] Zhang JF, Zhang XX, Andrä H, Wang QZ, Xiao BL, Ma ZY. A fast numerical method  
22 of introducing the strengthening effect of residual stress and strain to tensile behavior of  
23 metal matrix composites. *J Mater Sci Technol.* 2021;87:167-75.

- 1 [8] Zhang X, Zhao N, He C. The superior mechanical and physical properties of nanocarbon  
2 reinforced bulk composites achieved by architecture design - A review. *Prog Mater Sci.*  
3 2020;113:100672.
- 4 [9] Chen B, Kondoh K, Li J, Qian M. Extraordinary reinforcing effect of carbon nanotubes  
5 in aluminium matrix composites assisted by in-situ alumina nanoparticles. *Composites Part*  
6 *B.* 2020;183:107691.
- 7 [10] Liu ZY, Xiao BL, Wang WG, Ma ZY. Analysis of carbon nanotube shortening and  
8 composite strengthening in carbon nanotube/aluminum composites fabricated by multi-pass  
9 friction stir processing. *Carbon.* 2014;69:264-74.
- 10 [11] Liu ZY, Xiao BL, Wang WG, Ma ZY. Singly dispersed carbon nanotube/aluminum  
11 composites fabricated by powder metallurgy combined with friction stir processing. *Carbon.*  
12 2012;50(5):1843-52.
- 13 [12] Liu ZY, Xiao BL, Wang WG, Ma ZY. Developing high-performance aluminum matrix  
14 composites with directionally aligned carbon nanotubes by combining friction stir  
15 processing and subsequent rolling. *Carbon.* 2013; 62:35-42.
- 16 [13] Liu ZY, Xiao BL, Wang WG, Ma ZY. Modelling of carbon nanotube dispersion and  
17 strengthening mechanisms in Al matrix composites prepared by high energy ball  
18 milling-powder metallurgy method. *Composites Part A.* 2017; 94:189-98.
- 19 [14] Jiang L, Li Z, Fan G, Cao L, Zhang D. The use of flake powder metallurgy to produce  
20 carbon nanotube (CNT)/aluminum composites with a homogenous CNT distribution.  
21 *Carbon.* 2012; 50(5):1993-8.
- 22 [15] Tjong SC. Recent progress in the development and properties of novel metal matrix  
23 nanocomposites reinforced with carbon nanotubes and graphene nanosheets. *Mater Sci Eng*  
24 *R.* 2013;74(10):281-350.



- 1 [16] Zhang XX, Zhang JF, Liu ZY, Gan WM, Hofmann M, Andrä H, et al. Microscopic  
2 stresses in carbon nanotube reinforced aluminum matrix composites determined by in-situ  
3 neutron diffraction. *J Mater Sci Technol*. 2020;54:58-68.
- 4 [17] Bi S, Liu ZY, Yu BH, Ma GN, Wu LH, Xiao BL, et al. Superplastic deformation  
5 behavior of carbon nanotube reinforced 7055 Al alloy composites. *Mater Sci Eng A*.  
6 2020;797:140263.
- 7 [18] Bi S, Xiao BL, Ji ZH, Liu BS, Liu ZY, Ma ZY. Dispersion and Damage of Carbon  
8 Nanotubes in Carbon Nanotube/7055Al Composites During High-Energy Ball Milling  
9 Process. *Acta Metall Sin (Eng Lett)*. 2021;34(2):196-204.
- 10 [19] Dong S, Zhou J, Hui D, Wang Y, Zhang S. Size dependent strengthening mechanisms  
11 in carbon nanotube reinforced metal matrix composites. *Composites Part A*.  
12 2015;68:356-64.
- 13 [20] Bi S, Liu ZY, Xiao BL, Zan YN, Wang D, Wang QZ, et al. Enhancing  
14 strength-ductility synergy of carbon nanotube/7055Al composite via a texture design by  
15 hot-rolling. *Mater Sci Eng A*. 2021;806:140830.
- 16 [21] Ma K, Liu Z, Zhang X, Xiao B, Ma Z. Fabrication of high strength carbon  
17 nanotube/7055Al composite by powder metallurgy combined with subsequent hot extrusion.  
18 *Sci China Technol Sci*. 2021; 64:1081-91.
- 19 [22] Wei H, Li ZQ, Xiong DB, Tan ZQ, Fan GL, Qin Z, et al. Towards strong and stiff  
20 carbon nanotube-reinforced high-strength aluminum alloy composites through a  
21 microlaminated architecture design. *Scripta Mater*. 2014;75:30-3.
- 22 [23] Salama EI, Abbas A, Esawi AMK. Preparation and properties of dual-matrix carbon  
23 nanotube-reinforced aluminum composites. *Composites Part A*. 2017;99:84-93.
- 24 [24] Ma X, Huang C, Moering J, Ruppert M, Hoeppe HW, Goeken M, et al. Mechanical  
25 properties of copper/bronze laminates: Role of interfaces. *Acta Mater*. 2016;116:43-52.

- 1 [25] Zha M, Zhang HM, Yu ZY, Zhang XH, Meng XT, Wang HY, et al. Bimodal  
2 microstructure A feasible strategy for high-strength and ductile metallic materials. *J Mater*  
3 *Sci Technol.* 2018;34(2):257-64.
- 4 [26] Zhang J, Hao S, Jiang D, Huan Y, Cui L, Liu Y, et al. In situ synchrotron high-energy  
5 X-ray diffraction study of microscopic deformation behavior of a hard-soft dual phase  
6 composite containing phase transforming matrix. *Acta Mater.* 2017;130:297-309.
- 7 [27] Wu H, Fan G, Huang M, Geng L, Cui X, Chen R, et al. Fracture behavior and strain  
8 evolution of laminated composites. *Compos Struct.* 2017;163:123-8.
- 9 [28] Jiang L, Yang H, Yee JK, Mo X, Topping T, Lavernia EJ, et al. Toughening of  
10 aluminum matrix nanocomposites via spatial arrays of boron carbide spherical  
11 nanoparticles. *Acta Mater.* 2016;103:128-40.
- 12 [29] Fu X, Yu Z, Tan Z, Fan G, Li P, Wang M, et al. Enhanced strain hardening by bimodal  
13 grain structure in carbon nanotube reinforced Al–Mg composites. *Mater Sci Eng A.*  
14 2021;803:140726.
- 15 [30] Ma K, Liu ZY, Liu BS, Xiao BL, Ma ZY. Improving ductility of bimodal carbon  
16 nanotube/2009Al composites by optimizing coarse grain microstructure via hot extrusion.  
17 *Composites Part A.* 2021;140:106198.
- 18 [31] Liu ZY, Ma K, Fan GH, Zhao K, Zhang JF, Xiao BL, et al. Enhancement of the  
19 strength-ductility relationship for carbon nanotube/Al–Cu–Mg nanocomposites by material  
20 parameter optimisation. *Carbon.* 2020;157:602-13.
- 21 [32] Ma K, Liu ZY, Bi S, Zhang XX, Xiao BL, Ma ZY. Microstructure evolution and hot  
22 deformation behavior of carbon nanotube reinforced 2009Al composite with bimodal grain  
23 structure. *J Mater Sci Technol.* 2021;70:73-82.

- 1 [33] Ma K, Liu ZY, Liu K, Chen XG, Xiao BL, Ma ZY. Structure optimization for  
2 improving the strength and ductility of heterogeneous carbon nanotube/Al-Cu-Mg  
3 composites. *Carbon*. 2021;178:190-201.
- 4 [34] Fu X, Tan Z, Min X, Li Z, Yue Z, Fan G, et al. Trimodal grain structure enables  
5 high-strength CNT/Al-Cu-Mg composites higher ductility by powder assembly & alloying.  
6 *Mater Res Lett*. 2021;9(1):50-7.
- 7 [35] Shin SE, Bae DH. Fatigue behavior of Al2024 alloy-matrix nanocomposites reinforced  
8 with multi-walled carbon nanotubes. *Composites Part B*. 2018;134:61-8.
- 9 [36] Liao JZ, Tan MJ, Bayraktar E. Tension-Tension Fatigue Behaviour of Carbon  
10 Nanotube Reinforced Aluminium Composites. *Mater Sci Forum*. 2013;765:563-7.
- 11 [37] Shukla S, Komarasamy M, Mishra RS. Grain size dependence of fatigue properties of  
12 friction stir processed ultrafine-grained Al-5024 alloy. *Int J Fatigue*. 2018;109:1-9.
- 13 [38] Yogesha KK, Joshi A, Jayaganthan R. Fatigue Behavior of Ultrafine-Grained 5052 Al  
14 Alloy Processed Through Different Rolling Methods. *J Mater Eng Perform*.  
15 2017;26(6):2826-36.
- 16 [39] Nelson S, Ladani L, Topping T, Lavernia E. Fatigue and monotonic loading crack  
17 nucleation and propagation in bimodal grain size aluminum alloy. *Acta Mater*.  
18 2011;59(9):3550-70.
- 19 [40] Liu R, Tian YZ, Zhang ZJ, Zhang P, Zhang ZF. Fatigue strength plateau induced by  
20 microstructure inhomogeneity. *Mater Sci Eng, A*. 2017;702:259-64.
- 21 [41] Long J, Pan Q, Tao N, Dao M, Suresh S, Lu L. Improved fatigue resistance of gradient  
22 nanograined Cu. *Acta Mater*. 2019;166:56-66.
- 23 [42] Shao C, Zhang P, Wang X, Wang Q, Zhang Z. High-cycle fatigue behavior of TWIP  
24 steel with graded grains: breaking the rule of mixture. *Mater Res Lett*. 2019;7(1):26-32.

- 1 [43] Qian T, Karaman I, Marx M. Mechanical properties of nanocrystalline and  
2 ultrafine-grained nickel with bimodal microstructure. *Adv Eng Mater.*  
3 2014;16(11):1323-39.
- 4 [44] Lee YL, Pan J, Hathaway R, Barkey M. *Fatigue testing and analysis: theory and*  
5 *practice.* Elsevier: Butterworth-Heinemann, 2005.
- 6 [45] Fatemi A, Plaseied A, Khosrovaneh AK, Tanner D. Application of bi-linear log–log S–  
7 N model to strain-controlled fatigue data of aluminum alloys and its effect on life  
8 predictions. *Int J Fatigue.* 2005;27(9):1040-50.
- 9 [46] Pang J, Li S, Wang Z, Zhang Z. Relations between fatigue strength and other  
10 mechanical properties of metallic materials. *Fatigue Fract Eng Mater Struct.*  
11 2014;37(9):958-76.
- 12 [47] Wang AQ, Liu P, Xie JP, Wang WY, Li JW, Sun HL, et al. Interface characterization,  
13 precipitate evolution, and quantitative modeling of the microstructure/strength relationship  
14 in SiCp/2024Al composite. *Compos Interfaces.* 2015;22(9):847-66.
- 15 [48] Xue Y, El Kadiri H, Horstemeyer MF, Jordon JB, Weiland H. Micromechanisms of  
16 multistage fatigue crack growth in a high-strength aluminum alloy. *Acta Mater.*  
17 2007;55(6):1975-84.
- 18 [49] Yi JZ, Gao YX, Lee PD, Lindley TC. Effect of Fe-content on fatigue crack initiation  
19 and propagation in a cast aluminum–silicon alloy (A356–T6). *Mater Sci Eng A.*  
20 2004;386(1):396-407.
- 21 [50] Goswami R, Feng CR, Qadri SB, Pande CS. Fatigue-Assisted Grain Growth in Al  
22 Alloys. *Sci Rep.* 2017;7(1):1-7.
- 23 [51] Meyers MA, Mishra A, Benson DJ. Mechanical properties of nanocrystalline materials.  
24 *Prog Mater Sci.* 2006;51(4):427-556.